Osmotic pressure of suspensions comprised of charged microgels

A. Scotti [1], M. Pelaez-Fernandez,[2] U. Gasser,[3] and A. Fernandez-Nieves [2,4,5]

[1]*Institute of Physical Chemistry, RWTH Aachen University, 52056 Aachen, Germany*
[2]*Department of Condensed Matter Physics, University of Barcelona, 08028 Barcelona, Spain*
[3]*Laboratory for Neutron Scattering and Imaging, Paul Scherrer Institut, 5232 Villigen, Switzerland*
[4]*ICREA-Institucio Catalana de Recerca i Estudis Avancats, 08010 Barcelona, Spain*
[5]*School of Physics, Georgia Institute of Technology, Atlanta, 30332 Georgia, USA*

(Received 8 September 2020; accepted 8 December 2020; published 20 January 2021)

We determine the osmotic pressure of microgel suspensions using membrane osmometry and dialysis, for microgels with different softnesses. Our measurements reveal that the osmotic pressure of solutions of both ionic and neutral microgels is determined by the free ions that leave the microgel periphery to maximize their entropy and not by the translational degrees of freedom of the microgels themselves. Furthermore, up to a given concentration it is energetically favorable for the microgels to maintain a constant volume without appreciable deswelling. The concentration where deswelling starts weakly depends on the crosslinker concentration, which affects the microgel dimension; we explain this by considering the dependence of the osmotic pressure and the microgel bulk modulus on the particle size.

DOI: 10.1103/PhysRevE.103.012609

I. INTRODUCTION

Colloidal suspensions are comprised of Brownian particles, or colloids, dispersed in a liquid phase. Since the size ratio between the colloids and the solvent molecules is typically between 100 and 1000, it is reasonable to treat the liquid as a continuous medium with the colloidal particles dispersed in it. One can then think of the equation of state associated to the colloidal system, which, if sufficiently dilute, is nothing but the ideal gas law, often called Van't Hoff's law in the colloidal context: $\pi = \frac{N}{V} k_B T$, with π the osmotic pressure, N the particle number, V the accessible volume, k_B Boltzmann's constant, and T the absolute temperature. Note that π depends on the particle number density, $\rho = N/V$. In terms of the colloidal packing fraction, $\phi = v\rho$, with v the volume occupied by a single colloid, we can write the ideal gas law as $\pi = k_B T \phi / v$. This equation of state relates the three relevant state functions of the colloidal system, (π, ϕ, T), providing the basis for the analogy between colloidal and atomic systems that have spurred much of the colloidal science work in physics [1–10]. Obviously, as the particle density increases, π deviates from the ideal gas law. For hard spheres, the equation of state is the well-known Carnahan-Starling equation [11]. In the case, T only determines the thermal jiggling of the particles and is unable to induce phase transitions, which only occur via changes in ϕ.

Deviations from ideality also arise in the presence of other interparticle interactions, which can either be attractive or repulsive. An interesting example of this is provided by Brownian emulsions, which consist of thermal droplets dispersed in an immiscible continuous liquid phase. Below random close packing, corresponding to $\phi_{\rm rcp} \approx 0.64$, the osmotic pressure of the emulsion is well-described by a hard-sphere model, but in terms of an effective packing fraction accounting for the short-range interdroplet repulsion due to the surfactant stabilizing the droplets against coalescence [12]. Interestingly, despite $\phi_{\rm rcp}$ sets the largest achievable ϕ for hard spheres packed in a disordered state [13–15], emulsions can be compressed beyond random close packing. In this case, the droplets are forced to facet and become nonspherical; the scale of π is no longer set by $k_B T$ but rather by the energy density cost associated with deforming the drops. The osmotic pressure is then given by $\pi = \frac{\gamma}{a} f(\phi)$, where a is the drop radius, γ the interfacial tension, and $f(\phi)$ a function dependent only on packing fraction; π is then controlled by the Laplace pressure associated to the pressure jump at the droplet interface, $\Delta P \sim \frac{\gamma}{a}$, reflecting that increasing the droplet density in compressed emulsions occurs at the expense of the energy cost related to deforming the droplets [12,16–18].

As a second example, consider charged colloidal suspensions, which are comprised of colloids with a surface charge density and an associated electric double layer composed of counterions [19–22]; the colloid plus its double layer warrant electroneutrality. However, those counterions at the outskirts of the double layer that are weakly bounded to the particle, that is, with an attraction strength of order $k_B T$ or lower, can wander around the continuous phase, hence contributing to π. In this case, these counterions can no longer be considered as internal degrees of freedom of the colloid-double layer complex; the associated translational degrees of freedom of these ions then contribute to the suspension osmotic pressure. Indeed, early studies on the sedimentation of charged colloidal suspensions [23,24] clearly showed the existence of strongly inflated density profiles, which were qualitatively explained through the counterion contribution to π; the result was a gravitational length that was much larger than the one ex-

 ©2021 American Physical Society

pected if only the interacting charged colloids contributed to π.

Importantly, this ionic contribution to the osmotic pressure can have important consequences if the colloidal particles are compressible since, in this case, an unbalanced number of counterions between the inside and outside of the particles can result in an appreciable size change and hence in an associated change in the packing fraction of the suspension [25–33]. Microgels, which are cross-linked polymer networks in the colloidal-size domain, are an example of such compressible particles. Indeed, they are known to respond to external stimuli, including pH, T, solvent composition, or salt concentration by swelling or deswelling [34–39]. While in the deswollen state the particle bulk modulus, K_p, is comparable to that of hard-sphere-like colloids, in the swollen state, K_p can be significantly smaller [40]. Hence, in the limit where the suspension osmotic pressure, π, is smaller than K_p, the microgel particles will essentially retain their swollen volume, v_0. In contrast, for $\pi \geqslant K_p$, v will change in response to changes in the suspension osmotic pressure. Regrettably, the way v changes in this limit is hard to access experimentally; hence, the value of ϕ for suspensions comprised of compressible colloids is usually not known.

Alternatively, it is common to employ a generalized packing fraction, $\zeta = \rho v_0$, defined in terms of the particle volume in dilute suspensions, to parametrize particle number density and know whether the soft-aspects of the particles might be playing a role [10,29,41–44]; this is also usually done in computer simulations addressing the behavior of soft colloidal suspensions [33,45,46]. Clearly, $\zeta \neq \phi$, in general. At small particle densities, though, $v = v_0$ and $\zeta = \phi$.

In the literature, the generalized packing fraction of microgels at high particle number densities has been determined by measuring the viscosity of dilute microgel suspensions [27,30,42] or by using static light scattering [47]. Both these methods try to estimate the mass of a single microgel to then use it to compute the number of particles in solution. We previously showed that an alternative way to obtain ϕ at high particle number densities is to measure the suspension osmotic pressure [48]. We were then able to discuss the suspension phase behavior in terms of ϕ rather than ζ [41].

In this paper, we focus on the osmotic pressure itself, rather than on the fluid-crystal phase transition. We start by discussing what osmotic pressure is and how it can be measured. We then present details of how we actually measure it using both membrane osmometry and dialysis. We focus on how π depends on ζ and present a counterion-based model that allows describing our results for suspensions of ionic-microgels with varing crosslink concentration at packing fractions below random close packing. By assuming that at even higher packing fractions, π is still controlled by the counterions, we estimate ϕ in terms of ζ; this further allows obtaining how v changes with ϕ [48]. We then provide an improved version of the same model and discuss how particle compression, which is the defining key difference between microgels and say emulsion droplets or conventional hard colloids, affects the osmotic pressure of the suspension. We end the paper by concluding and providing a few final remarks on aspects and questions that could perhaps be tackled in the future either theoretically or using computer simulations.

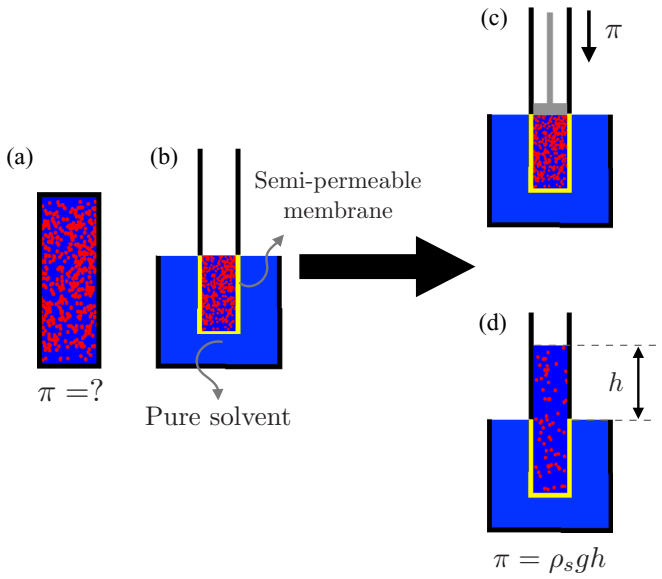

FIG. 1. (a) Sketch of a solute-solvent mixture whose osmotic pressure π we want to know. (b) Sketch of the solute-solvent mixture in contact with a pure solvent reservoir *via* a semipermeable membrane. (c) Sketch of a piston compressing the solute-solvent mixture that is in contact with the pure solvent reservoir *via* a semipermeable membrane. The exerted pressure is the osmotic pressure π. (d) Sketch of the solute-solvent mixture in contact with the pure solvent reservoir *via* a semipermeable membrane in the absence of the piston in (c). In this case, equilibrium is achieved after pure solvent flows into the mixture to result in a hydrostatic pressure $\rho_s g h$, with ρ_s the density of pure solvent, g the acceleration of gravity, and h the height change of the free surface of the solute-solvent mixture; this hydrostatic pressure exactly equals the osmotic pressure π of the solute-solvent mixture.

II. OSMOTIC PRESSURE: DEFINITION AND FUNDAMENTALS

The osmotic pressure of a solute-solvent mixture, such as that illustrated in Fig. 1(a), is the extra pressure required to equilibrate the mixture with pure solvent. To determine π, we introduce our sample in a pure solvent reservoir and allow their coupling via a semipermeable membrane, as shown in Fig. 1(b). The pressure required to equilibrate the system is the osmotic pressure of the mixture; it is the pressure applied to the piston in the schematic shown in Fig. 1(c). Alternatively, we can allow solvent through the membrane into the mixture, as schematically shown in Fig. 1(d). In this case, the extra pressure required to establish equilibrium equals the gravitational potential energy, per unit volume, of the pure solvent that moved inside the mixture: $\pi = \rho_s g h$, with ρ_s the solvent density, g the acceleration of gravity, and h the difference in height between the free surface of the mixture and that of the pure solvent.

Since solvent flow through a semipermeable membrane is involved in defining the osmotic pressure of a mixture, it is not surprising that it can be related to the chemical potential of the

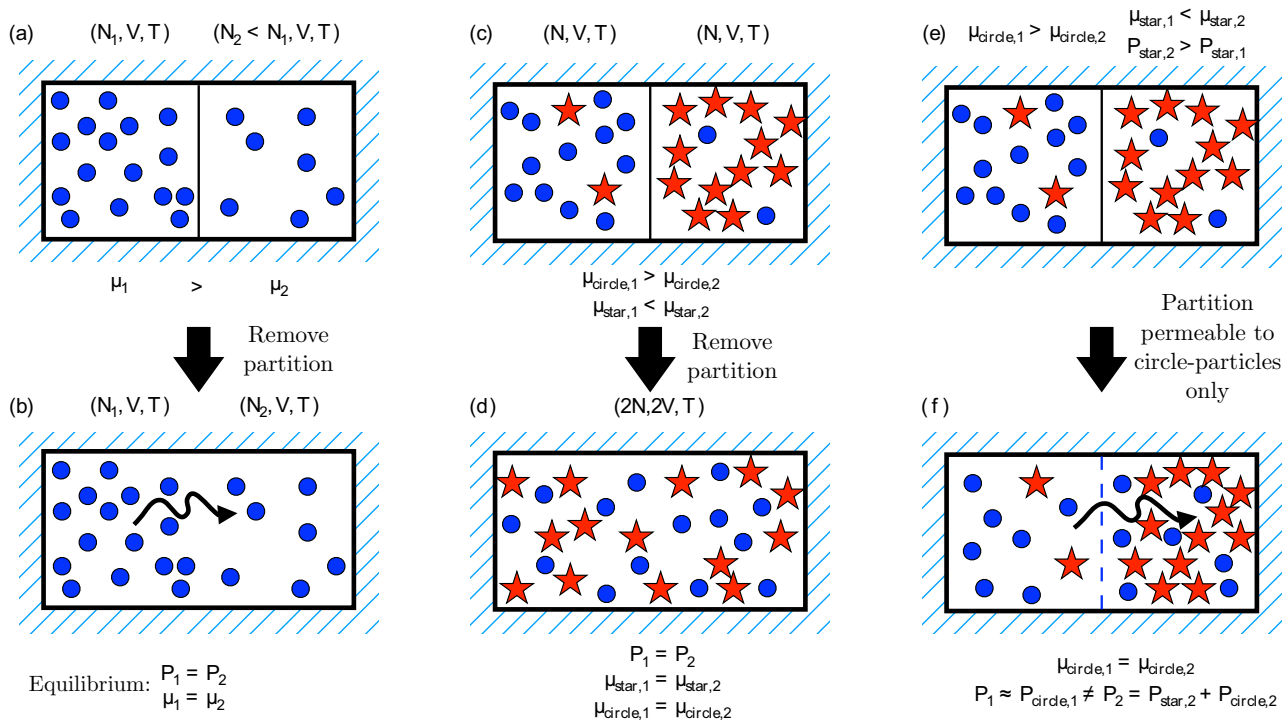

FIG. 2. (a) Sketch of two fluids comprised of identical particles (circles) separated by a partition (vertical line). There is a different number of particles to each side of the partition. (b) Same as in (a) but after removing the partition. The arrow represents the flow direction. In equilibrium, the intensive parameters match and thus $P_1 = P_2$ and $\mu_1 = \mu_2$. (c) Sketch of two fluids comprised of different particles, stars, and circles. The two fluids are separated by a partition (vertical line). There are more circle particles on side 1 than on side 2, and more star particles on side 2 than on side 1. The total number of particles on either side is N. (d) Same as in (c) after removing the partition and once equilibrium is reached. In this situation, the pressure, and the chemical potential of both species, match. (e) Same as in (c), but now instead of removing the partition, we make it permeable to circle-particles only. (f) Equilibrium situation reached, where only the chemical potential of the circle particles matches at either side of the semipermeable membrane. The arrow represents the flow direction of these particles before equilibrium is established. In this case, $\mu_{\text{circle},1} = \mu_{\text{circle},2}$ but $P_1 \neq P_2$ and $\mu_{\text{star},1} \neq \mu_{\text{star},2}$.

solvent [49]. To clearly grasp the significance of this connection, let us review some aspects of the chemical potential, μ, of classical systems.

Consider a (P, V, T, N) system, where P is the intensive variable conjugate to the extensive variable V; these are the pressure and volume, respectively, for a fluid system. The Gibbs equation in the energy representation then is $dE = TdS - PdV + \mu dN$. It follows that $\mu = (\frac{\partial E}{\partial N})_{S,V}$; the chemical potential of the system is the rate of change of its energy with the number of particles at constant entropy S and constant V. This expression, despite its phenomenological character, is a powerful definition with which to think and understand what the chemical potential is. The key is that particle addition or extraction is done at constant entropy. For a classical system, adding a particle increases the number of microstates and hence its entropy; this is familiar to us in the context of ideal gases, since $S \sim V^N$ in this case, but it is generally true for any classical system. Note that since in the process V is held constant, there is no work involved and the energy has not yet changed. However, to comply with the constant entropy condition, we must lower the entropy; this is done by releasing heat, which as a result, causes the energy of the system to decrease. Hence, for classical systems $\mu < 0$.

Now, let's recall some basic statistical mechanics. In general, we know that $\mu = k_B T \ln z$, with z the fugacity. For ideal gases, $\ln z = \ln \rho + \ln \lambda_t^3$, with ρ the density and λ_t the thermal de Broglie length. Recall that the loss in ideality amounts to, at the thermodynamic level, a prefactor inside the natural logarithm containing the λ_t term; this is sometimes called an activity coefficient.

We are now ready to consider mass transfer between systems. We start with the simple case of two fluids comprised of identical particles separated by a partition, each occupying the same volume and at the same temperature, but with a different number of particles; assume $N_1 > N_2$, implying that $\mu_1 > \mu_2$, as illustrated in Fig. 2(a). If we now remove the partition, since the composite system is isolated from the surroundings, the maximum entropy principle requires that particles in regions of high chemical potential flow to regions of low chemical potential, as illustrated in Fig. 2(b). Equilibrium is reached when S is maximum, corresponding to $P_1 = P_2$ and $\mu_1 = \mu_2$.

As a natural next step, let's focus on two-component systems and consider two-fluid mixtures separated by a partition. We represent each fluid with circles and stars, as shown in Fig. 2(c), and consider that each initially occupies the same volume and are at the same temperature, but that the number of stars on side 1 is much smaller than on side 2 and, likewise, that the number of circles on side 1 is much larger than that of side 2. Hence, initially, $\mu_{\text{star},1} < \mu_{\text{star},2}$ and $\mu_{\text{circle},1} > \mu_{\text{circle},2}$. Removing the partition results in star particles moving to side

1 and circle particles moving to side 2; each flows toward regions of lower chemical potential. At equilibrium, $P_1 = P_2$, $\mu_{\text{star},1} = \mu_{\text{star},2}$ and $\mu_{\text{circle},1} = \mu_{\text{circle},2}$; see Fig. 2(d).

Now, if instead of removing the partition, we make it permeable only to the circle particles, these will be the ones flowing from side 1 to side 2 to reestate equilibrium, as schematically shown in Figs. 2(e) and 2(f). In this case, at equilibrium, $\mu_{\text{circle},1} = \mu_{\text{circle},2}$ but $P_1 \neq P_2$. Instead, $P_1 \approx P_{\text{circle},1}$, where we neglect the small number of star particles on side 1, and $P_2 = P_{\text{star},2} + P_{\text{circle},2}$, where we have assumed that the two fluids are weakly coupled; the resultant pressure difference is balanced by the rigid walls of the container and exactly corresponds to the additional pressure that is needed to equilibrate the system in the presence of mass transfer via a semipermeable membrane. Note that if the fluids were ideal, the partial pressure of the circle particles would be equal at equilibrium. In this case, $P_1 \approx P_{\text{circle},1} = P_{\text{circle},2} \neq P_2 = P_{\text{circle},2} + P_{\text{star},2}$, and the osmotic pressure $\pi = P_2 - P_1 = P_{\text{star},2}$.

The connection with the solute-solvent mixtures that we are interested in can easily be made if we take the circle particles to be the solvent and the star particles to be the solute. Assuming in this case that the solute and the solvent are weakly coupled, we then see that the osmotic pressure is simply $\pi = P_2 - P_1$. This result further illustrates that the extra pressure required to equilibrate the system is nothing but the pressure associated to the solute particles, which are those that cannot flow through the semipermeable membrane.

We are now in a position to connect π and the chemical potential of the solvent, μ_s. The starting point is the equilibrium condition, corresponding to the equality of the chemical potential of the solvent at both sides of the semipermeable membrane,

$$\mu_s^{\text{pure}}(P, T) = \mu_s(P + \pi, T), \tag{1}$$

where μ_s^{pure} is the chemical potential of the pure solvent. It is customary to introduce the notion of the excess chemical potential, $\Delta\mu_s = \mu_s(P, T) - \mu_s^{\text{pure}}(P, T)$, relating the chemical potential of the solvent in the mixture relative to that of the pure solvent. We then use that

$$\mu_s^{\text{pure}}(P + \pi, T) \; - \; \mu_s^{\text{pure}}(P, T) = \int_P^{P+\pi} \left(\frac{\partial \mu_s^{\text{pure}}}{\partial P'} \right)_T dP' \; = \; v_s \, \pi, \tag{2}$$

where in the last step we have used the Gibbs-Duhem equation and thus that the volume per particle of pure solvent is $v_s = \frac{V}{N} = (\frac{\partial \mu_s^{\text{pure}}}{\partial P})_T$. Combining this last equation with Eqs. (1) and (2) yields the relation that formally relates the osmotic pressure to the chemical potential of the solvent:

$$\pi = -\frac{\Delta\mu_s}{v_s}. \tag{3}$$

Since the solvent flows toward regions of lower chemical potential, the minus in Eq. (3) indicates that the solvent flows toward regions of larger π. Furthermore, since π is directly related to the pressure exerted by the solute, we see that the solvent will flow toward regions where the number density of the solute is largest.

TABLE I. Microgel suspensions used in this paper. The labels VP and p stand for ionic microgels comprised of 2-vinylpyridine and for neutral microgels comprised of pNIPAM, respectively. The crosslinker concentration, and swollen and deswollen diameters, measured by dynamic light scattering, are c_X, d, and d_d, respectively. We also provide the generalized packing fraction ζ_f above which the suspension crystallizes.

Label	c_X (wt. %)	d (nm)	d_d (nm)	ζ_f
VP1 □	0.2	1050 ± 21	183 ± 3	-
VP2 ○	0.5	1020 ± 21	185 ± 5	1.9 ± 0.1
VP3 △	1.3	705 ± 8	177 ± 2	1.05 ± 0.05
VP4 ▽	1.6	701 ± 13	181 ± 2	0.87 ± 0.04
VP5 ◇	1.8	634 ± 8	177 ± 9	0.76 ± 0.03
VP6 ◁	2.5	545 ± 7	186 ± 3	0.65 ± 0.04
p1 ○	2.0	240 ± 3	79 ± 1	-
p2 □	2.0	280 ± 3	71 ± 2	0.58 ± 0.02

III. MATERIALS AND METHODS

A. Experimental system

Our microgel particles are comprised of 2-vinylpyridine (2VP) and crosslinker divinylbenzene, and are immersed in water [35]. Their swelling behavior can be controlled via the suspension pH. For sufficiently low pH, the 2VP groups ionize, drawing counterions to the inside of the particles. This raises the internal osmotic pressure driving solvent into the microgels and causing their swelling. The equilibrium size results from the balance between this ionic osmotic pressure and the elastic stress associated to the crosslinked network [40,50]. We quantify the swelling behavior using multiangle dynamic light scattering [51], finding that for pH < 3.3, all studied microgels are completely swollen, while they are deswollen for pH > 4.5 [41]. Swollen and deswollen diameters are shown in Table I for microgels with different crosslinker concentration, c_X; we see that the swollen size d increases as c_X decreases, confirming the role of the crosslinker in determining swelling equilibrium, while the deswollen size d_d remains essentially the same. We also note that for 2VP microgels, d_d at high pH is comparable to the collapsed size d_c [52]; hence, the swollen-to-collapsed volume ratio $\alpha = (\frac{d}{d_c})^3 \approx (\frac{d}{d_d})^3$. For 2VP microgels with $c_X = 0.2\%$ and synthesized using the same protocol as those used here, the network charge is $Q = 5 \times 10^6$ e$^-$, as obtained by titration at pH $= 3$ [52]. Since the total solid fraction resulting from the synthesis of microgels with different c_X is always $\approx$1%, and c_X is 2.5 wt. % at most, Q is essentially the same at pH $= 3$ irrespective of c_X.

We emphasize that despite in the swollen state the microgels are most ionized, the effective charge per particle is small due to the presence of counterions inside the particles. As a result, the repulsive interaction between microgels is weak and the particles only appreciably interact when their interparticle distance is comparable to or smaller than d. Consequently, they behave as soft spheres. In fact, our microgel suspensions freeze at packing fractions ζ_f larger than that for hard-sphere suspensions; ζ_f is thus always larger than 0.49 [1], as shown in Table I. Suspensions are prepared from a concentrated stock suspension by dilution to the wanted generalized packing frac-

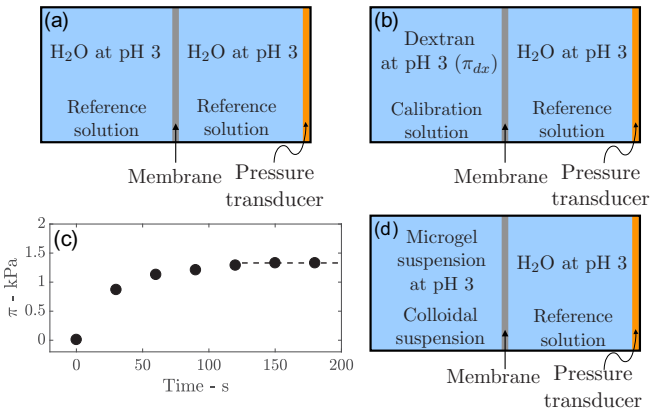

FIG. 3. Schematic of the membrane osmometer in the (a) *setting the zero* and (b) *calibration* stages. (c) Osmotic pressure readings after subsequent injections in a typical calibration. The dashed line indicates the stationary value, which is the one we take as the definite osmotic pressure value. (d) Schematic of the membrane osmometer in the measurement stage.

tion ζ, which we can relate to the density of the 2VP polymer ρ_0, the solvent density ρ_s, the polymer weight fraction in the suspension c, and the size ratio α, using $\zeta = \frac{\rho_s}{\rho_0} c\,\alpha$. Since $\rho_s/\rho_0 = 0.97 \approx 1$ [52], $\zeta \approx c\,\alpha$. The pH of the suspensions is fixed by adding a few drops of concentrated HCl.

We also use poly-N-isopropilacrylamide (pNIPAM) microgels; these are synthesized by well-established precipitation polymerization techniques [37,53], where a crosslinker [N, N'-methylenebis(acrylamide), BIS, 2 wt %] is added to the monomer and the reaction initiated using ammonium persulfate (APS) [29,30]. Sodium dodecyl sulfate (SDS) is used to finely control both the final size and the size polydispersity of the resulting microgel suspension [54]. Prior to use, the suspensions are extensively dialyzed to remove the surfactant and any unreactant monomers.

B. Membrane osmometry

We use a commercial membrane osmometer (Wescor 4200 Colloid Osmometer) to measure the osmotic pressure of microgel suspensions. The apparatus consists of two chambers separated by a semipermeable membrane. The pore size of the membrane is ∼50 nm. The chambers to either side of the membrane have a volume of ≈350 μl. One of them is coupled to a pressure transducer that allows converting the mechanical pressure into an electrical signal, which is then transformed into a pressure value. The experimental procedure is the following:

(i) Setting the zero: We first fill both chambers with the same solution, which we call the reference solution, as illustrated in Fig. 3(a). In the work presented here, we use deionized (DI) water at pH = 3.0 as our reference solution. We add ∼50 μL of reference solution, allow 30–90 seconds for the osmometer reading to equilibrate, and repeat the process until the reading remains stationary. We associate an osmotic pressure of zero to the reading of the transducer in these conditions.

(ii) Calibration: We keep the chamber in contact with the transducer with the same reference solution and fill the other chamber with a polymer solution of known osmotic pressure, as schematically shown in Fig. 3(b). We use Dextran T110 in DI water at pH = 3.0. The osmotic pressure of this polymer solution, noted as π_{dx}, is well-known [55,56]. We proceed as before and progressively introduce the dextran solution until a steady-state reading is obtained. This typically happens after four or five injections, as shown in Fig. 3(c). We then calibrate the transducer reading to the known value of π_{dx}.

(iii) Confirming the zero: We remove the dextran solution from the corresponding chamber and replace it with the reference solution to confirm that the osmotic pressure reading is zero, as it should be.

(iv) Measurement: We introduce the microgel suspension and determine the suspension osmotic pressure with respect to the reference solution used in the calibration stage; this is schematically illustrated in Fig. 3(d). Note that the pH of the reference solution, the dextran solution, and the microgel suspension is always 3.0. This assures that the π we measure for the microgel suspension does not include the contribution from the excess ions required to set the pH to 3.0.

C. Dialysis

We also determine the suspension osmotic pressure using dialysis. The dialysis tubing we employ (Spectra/Por 2, Spectrum) has a quoted cutoff molecular weight of ∼13 kD. Prior to use, the tubing is introduced in deionized water and brought to a temperature slightly below the boiling point of water for a few seconds to remove undesired iodine ions [57]. This process is repeated at least three times. Once cleaned, the dialysis tubing is filled with the microgel suspension at pH = 3.0 and at a generalized volume fraction ζ_0, corresponding to an initial osmotic pressure π_0. The sample is then introduced in a dextran solution of known osmotic pressure π_{dx}; see Fig. 4(a) and 4(b). Since the volume ratio between the external dextran solution and the microgel suspension is >100, the dextran solution effectively acts as a particle reservoir. As a result, at equilibrium, the osmotic pressure of the microgel suspension is $\pi = \pi_{dx}$. In contrast, the value of ζ will, in general, differ from ζ_0.

IV. RESULTS AND DISCUSSION

A. Dialysis results

The time for the microgel suspension to equilibrate with the dextran solution depends on the osmotic pressure difference $\pi_0 - \pi_{dx}$. For a microgel suspension at the same ζ_0, the time-dependence of the weight fraction c is more pronounced for $\pi_{dx} = 50$ kPa than for $\pi_{dx} = 2.5$ kPa, as shown in Fig. 5(a) with squares and circles, respectively. In both these cases, $\pi_{dx} > \pi_0$ and thus the solvent flows out of the dialysis tubing, causing c to increase. If, alternatively, we had $\pi_{dx} < \pi_0$, solvent would flow into the dialysis tubing causing c to decrease.

Equilibrium is reached when $\pi = \pi_{dx}$. Note that in this state, there are suspensions found in fluid or crystalline states, as shown in Figs. 4(c) and 4(d). To determine c, we use gravimetric analysis [41]; we carefully extract the dialysis bags from the dextran reservoir and perform the necessary

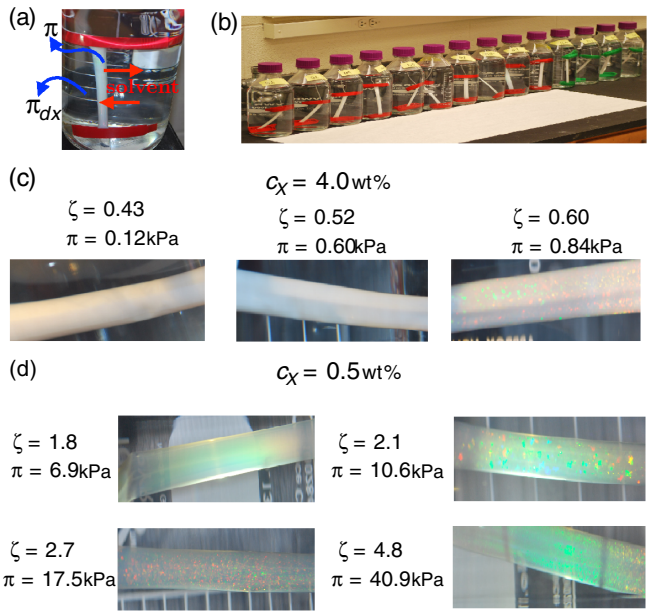

FIG. 4. (a) Dialysis bag (white) immersed in a dextran solution reservoir. Red arrows indicate that solvent can be exchanged depending on the osmotic pressure π_0 of the sample in the dialysis bag and of the dextran solution π_{dx}. (b) Series of microgel suspensions immersed in dextran solutions. (c,d) Microgel suspensions synthesized with $c_X = 4.0$ wt. % and $c_X = 0.5$ wt. %. The microgel suspensions in the dialysis bags are in either a disordered or in a crystalline phase. On top of every image we indicate the generalized volume fraction, ζ, and the osmotic pressure, π, of the microgel suspensions at equilibrium.

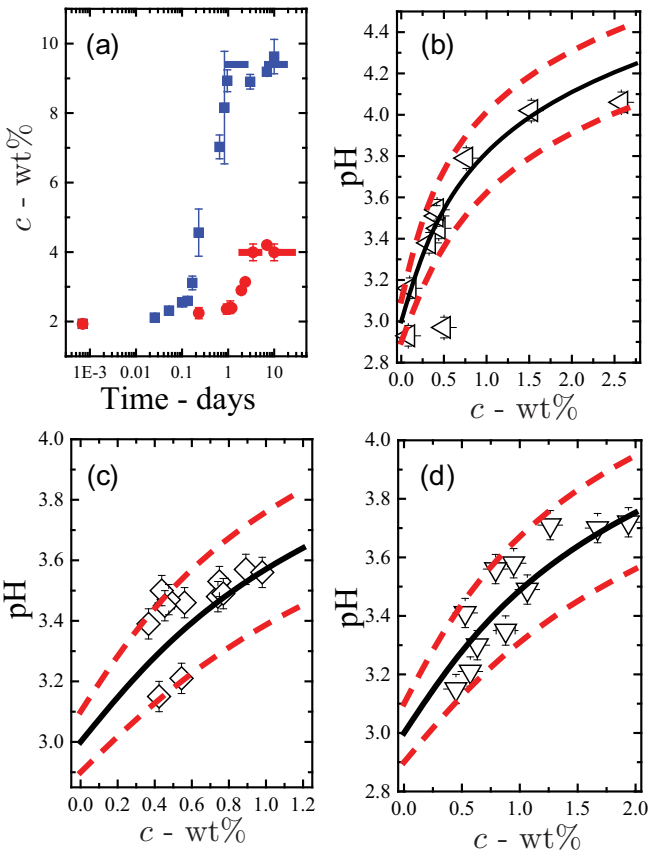

FIG. 5. (a) Polymer weight fraction c of a microgel suspension inside the dialysis tubing as a function of the time inside dextran reservoirs at osmotic pressures $\pi_{dx} = 2.5$ kPa (circles) and $\pi_{dx} = 50$ kPa (squares). The dashed lines indicate that equilibrium has been attained. (b) Suspension pH versus c for samples (b) VP4, (c) VP5, and (d) VP6. Black solid lines represent the prediction from Eq. (6) using $f = 0.8$ and $[H^+]_{\text{out}} = 1$ mM. The dashed lines are the predictions for $[H^+]_{\text{out}} = 2.9$ (upper curve) and $[H^+]_{\text{out}} = 3.1$ (lower curve), corresponding to the error in our pH measurements.

mass measurements. From c, we calculate ζ using the size ratio α. We also measure the suspension pH.

Interestingly, we always find that the suspension pH >3.0, as shown with symbols in Figs. 5(b)–5(d) for microgels with $c_X = 1.6\%$, $c_X = 1.8\%$, and $c_X = 2.5\%$, respectively. We also see that the equilibrium pH increases with c. In constrast, the pH of the particle reservoir remains equal to 3.0, as expected. To understand this result we recall that the dialysis tubing is permeable to both the solvent and the ions. Hence, at equilibrium,

$$\ln([H^+]_{\text{in}}) + \ln([OH^-]_{\text{in}} + [Cl^-]_{\text{in}}) = \ln([H^+]_{\text{out}}) + \ln([OH^-]_{\text{out}} + [Cl^-]_{\text{out}}) \quad (4)$$

where we have treated the ions (H^+, OH^-, and Cl^-) as an ideal gas. The subindeces *in* and *out* refer to inside and outside the dialysis tubing, respectively. We further impose electroneutrality on both sides of the dialysis tubing, and thus

$$[H^+]_{\text{in}} + f \cdot [M] = [OH^-]_{\text{in}} + [Cl^-]_{\text{in}}, \quad [H^+]_{\text{out}} = [OH^-]_{\text{out}} + [Cl^-]_{\text{out}} \quad (5)$$

where f represents the fraction of ionized monomer inside the microgel particle and $[M]$ is the total concentration of ionizable groups. We estimate $[M]$ from c and the molecular weight of the 2VP monomer, $M_w = 105.14$ g/mol, assuming that the density of swollen microgel suspensions is equal to the solvent density: $[M] = \frac{\rho_s c}{M_w}$. Combining Eqs. (4) and (5), we can solve for $[H^+]_{\text{in}}$:

$$[H^+]_{in} = \tfrac{1}{2}\left(- f \cdot [M] + \sqrt{(f \cdot [M])^2 + 4[H^+]^2_{\text{out}}}\right). \quad (6)$$

The associated pH is $\text{pH}_{\text{in}} = -log_{10}([H^+]_{\text{in}})$. We now use that $\text{pH}_{\text{out}} = -\log_{10}([H^+]_{\text{out}}) = 3.0$ and fit pH_{in} versus c using Eq. (6), with f as a fitting parameter. The solid lines in Figs. 5(b) and 5(d) are the results from the fit and describe the experimental results reasonably well. We find $f \approx 0.8$ in all cases, reflecting that at these pHs, the number of 2VP groups in the particles that are ionized is high. The dashed lines in Figs. 5(b-d) are the expectations from Eq. (6) for $f = 0.8$ also, but with $\text{pH}_{\text{out}} = 2.9$ or $\text{pH}_{\text{out}} = 3.1$, which account for the experimental uncertainty in pH_{out}. The data points all lie within these lines. We emphasize, however, that as pH_{in} increases, we expect f to decrease. Our model bypasses this fact by fixing a value of f that is high, but not 1, to reach a compromise to the possible f variation.

More importantly, our model provides the option to set the value of pH_{out} such that at equilibrium $\text{pH}_{\text{in}} = 3.0$; this is a desirable aspect if we want to obtain π at fixed pH_{in}. Our

model thus provides the way to adjust pH_{out} to obtain how π depends on ζ at a fixed pH of say 3.0.

In addition, these experiments and our modeling confirm that the suspension is locally electroneutral and that the counterions that are able to leave the microgel, because they may be attracted with a strength of order k_BT, remain within the vicinity of where the microgel particles are [24,58]. They do not leave, for instance, to the dextran reservoir outside the dialysis bag; at most, they might exchange with other equally charged ions. This further implies that in the membrane osmometry experiments, the number of counterions does not change, remaining essentially constant in the chamber where the microgel suspension is located. Hence, by fixing the pH to 3.0 on both sides of the membrane, we assure we measure the suspension osmotic pressure without the contribution from the ions used to set up the pH value of the samples.

B. Osmotic pressure of ionic microgel suspensions

The osmotic pressure determined via membrane osmometry versus ζ for all VP microgels in Table I is shown in Figs. 6(a-f). The experimental ζ range explored spans from ~0.01 to ~3 and includes fluid, fluid-crystal coexistence, and crystalline phases. We also measure π using dialysis. In this case, we use Eq. (6) to calculate pH_{out} so the equilibrium pH inside the dialysis tubing is 3.0. We find that the dialysis (crossed symbols) and membrane osmometry experiments compare well in the ζ range where these overlap, as shown in Figs. 6(a)–6(f) for 2VP microgels with different c_X. Note that we plot the dimensionless pressure $\frac{\pi v_0}{k_BT}$ versus ζ, as for hard sphere suspensions $\frac{\pi v_0}{k_BT}$ is a universal function of ϕ.

In the dilute limit, where ideal behavior must hold, $\pi = \frac{k_BT}{v_0}\zeta$. However, if, for example, we consider VP microgels with $c_X = 2.5\%$, we have $v_0 = 4 \times 10^{-20}$ m^3 and would expect $\pi \sim 2$ Pa at $\zeta = 0.01$. In contrast, we find that the measured osmotic pressure is more than three orders of magnitude larger. Additionally, in this low concentration regime and based on ideal gas expectations, $\pi \propto \frac{\zeta}{v_0}$ [48]; we also do not observe this experimentally. These results suggest that the origin of π in our suspension is not related to the translational degrees of freedom of the microgel particles. Since the only other particles that can potentially contribute are the free ions in solution, we then consider an ionic microgel and its associated counterions [25]. Due to the size difference between the microgel and the counterions, one can think of the charge on the polymer network in terms of a Donnan potential that decays to zero in the vicinity of the particle (see Fig. 7). This decay defines a characteristic length scale $\kappa^{-1} = \sqrt{\frac{(d/2)^3}{2l_BQ}}$, where l_B is the Bjerrum length, and implies that some of the counterions that are required to assure electroneutrality will be attracted to the microgel particle with a strength of order of k_BT. These ions can then escape from the particle for entropic reasons and contribute to the suspension osmotic pressure. We estimate the fraction, Γ, of these ions as [25]

$$\Gamma = \frac{\left(\kappa^{-1} + \frac{d}{2}\right)^3 - \left(\frac{d}{2}\right)^3}{\left(\frac{d}{2}\right)^3} \approx 6\frac{\kappa^{-1}}{d} = \frac{3}{2}\sqrt{\frac{d}{l_BQ}}, \qquad (7)$$

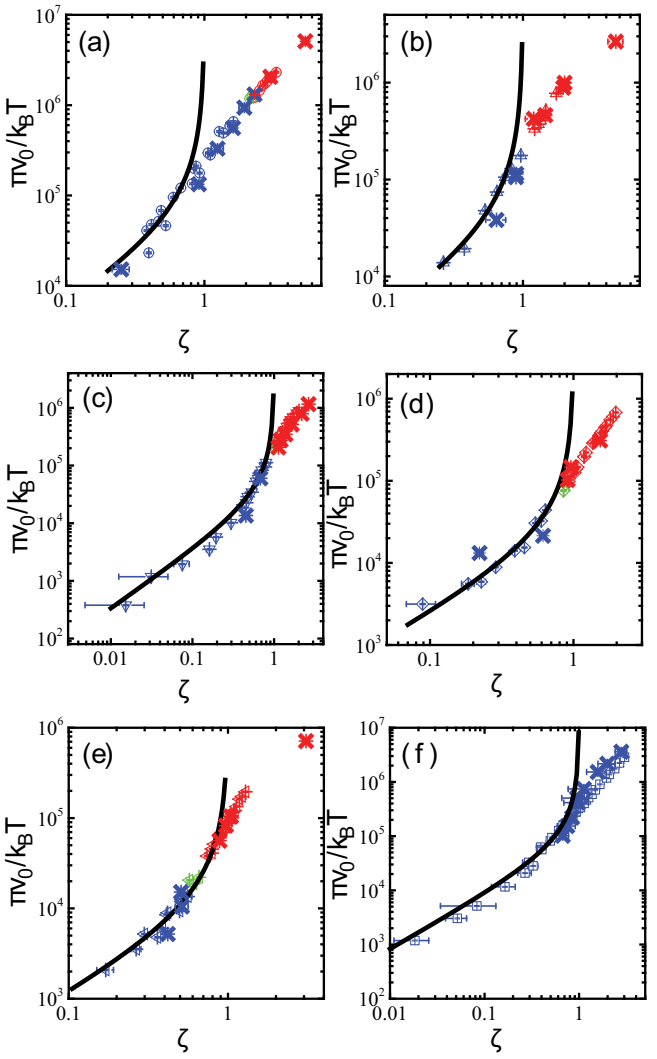

FIG. 6. (a-f) Normalized osmotic pressure versus ζ corresponding to samples VP1–VP6. Symbols represent experimental data from membrane osmometry (noncrossed symbols) and dialysis (crossed symbols). The solid line is the best fit to Eq. (8) for $\zeta < 0.63$.

where we have used that $\kappa^{-1} << d$. By treating these ions as an ideal gas, we can write their contribution to the suspension osmotic pressure in terms of the microgel volume fraction:

$$\pi_c(\phi) = k_BT\frac{\Gamma QN}{V - Nv_0} = k_BT\frac{\Gamma Q}{v_0}\frac{\phi}{1-\phi}, \qquad (8)$$

where ΓQ is the number of free counterions per microgel contributing to π and $V - Nv_0$ is the volume that is available to them; note that it is ϕ that enters in Eq. (8). Considering that $\phi \approx \zeta$ for $\zeta \lesssim 0.63$, we can fit the data in Figs. 6(a-f) with ΓQ as a free parameter. We find that the model describes the experiment. Furthermore, ΓQ is well described by Eq. (7) [48].

Interestingly, this ionic contribution also determines the osmotic pressure of pNIPAM microgel suspensions. In contrast to VP microgels, pNIPAM microgels are considered neutral, since their swelling is not affected by variations of the suspension pH. The pNIPAM microgels used here all have a similar

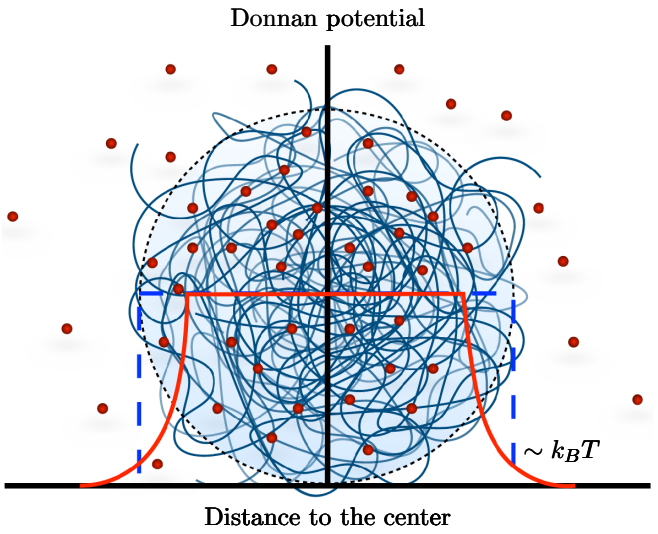

FIG. 7. Illustration of the Donnan potential inside a swollen ionic microgel and its smooth decay at the outer regions of the particle.

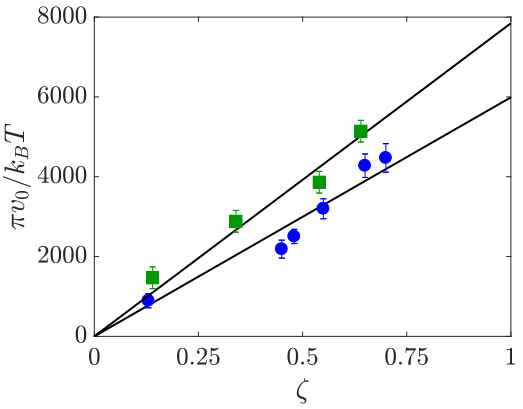

FIG. 8. Normalized osmotic pressure versus ζ for pNIPAM microgel suspensions comprised of particles with a diameter of 240 nm (circles) and 280 nm (squares). The lines are linear fits to the data according to Eq. (10).

mass, $m_p \approx 6.4 \times 10^{-16}$ g [29], and are synthesized via precipitation polymerization using a constant amount of initiator, $m_{\rm APS} = 0.228$ g. The molecular weight of APS, $(NH_4)_2S_2O_8$, is $M_{\rm APS} = 228$ g/mol. Now, since these neutral pNIPAM microgels contain SO_3^- groups, which originate from the initiator, residing at the periphery of the particles [53], there must be an equal number of NH_4^+ counterions in solution due to electroneutrality. The total number of counterions per particle can be estimated as

$$Q_{\rm pNIPAM} = 2\frac{N_A m_p m_{\rm APS}}{m M_{\rm APS}} = 6.8 \times 10^4 , \qquad (9)$$

where $m = 11.33$ g is the total mass of all reactants used in the synthesis and $N_A = 6.022 \times 10^{23}$ mol^{-1} is Avogadro's number. The quantity $m_p m_{\rm APS}/m$ represents the fraction of APS incorporated per microgels, and the 2 in the prefactor accounts for the fact that every molecule of APS has 2 associated NH_4^+ counterions.

These counterions are located mainly in a double layer at the particle periphery; those attracted with an energy $\lesssim k_BT$ can leave the microgel. Assuming these ions behave as an ideal gas, we expect that for low-ζ values, the osmotic pressure would increase linearly with ζ and that the slope of the line is related to the number of free counterions in suspension:

$$\frac{\pi v_0}{k_B T} = Q_{\rm free}\zeta . \qquad (10)$$

As an example, we plot in Fig. 8 the values of the osmotic pressure π measured using membrane osmometry for two suspensions of pNIPAM microgels, p1 (blue circles), and p2 (green squares); in the swollen state the diameters of these microgels are 240 and 280 nm, respectively. Both microgels are synthesized with $c_X = 2$ wt %. In these measurements, the reference solution was deionized water at pH = 7.0 and 20 °C. By comparing the results of the measurements in Figs. 6 and 8, we find that the osmotic pressure values of the pNIPAM and 2VP microgel suspensions are of the same order of magnitude. In contrast to the suspensions of 2VP microgels, however, π increases linearly with ζ for the pNIPAM microgel suspensions.

The solid black lines in Fig. 8 represent linear fits of the data. From the slope of the fits, we find $Q_{{\rm free},p1} = (6.0 \pm 0.7) \times 10^3$ and $Q_{{\rm free},p1} = (8 \pm 1) \cdot 10^3$. This indicates that for both pNIPAM microgels, the counterions that leave the particle are ≈10% of the total, consistent with previous findings [29].

The observed linearity in the probed ζ range can be understood from the fact that, in contrast to ionic microgels, pNIPAM microgels have a neutral network and thus there is no Donnan potential; the ions can then locate both inside and outside the particles [29,30,59]. Increasing the particle number density proportionally increases the number of free ions per particle, and since these can explore the inside and outside of the microgels, π should increase linearly with ζ.

The picture that emerges is that inside the VP microgels, which posses a charged network that in the continuum limit result in a Donnan potential, there are strongly bound counterions. At the interface of the microgels, however, there is an electric double layer with some weakly bound counterions that are able to escape to increase their entropy; these ions seem to control the osmotic pressure of the suspension. This results in an unbalance of charges producing an effective charge. Note that this effective charge is small relative to the network charge; we find there are $O(10^3)$ ions that contribute to π, while the network charge Q is $O(10^6)$. The fact that Γ is $O(10^{-3})$ explains (i) why the swelling of individual microgels is correctly described by assuming the microgel is electroneutral when these are in dilute suspension [27,52,60] and (ii) why the osmotic pressure of these effectively free ions overwhelms the contribution associated to the translational degrees of freedom of the particles, as there are $O(10^3)$ ions that escape per microgel particle.

Interestingly, the existence of an effective charge enables looking at our results from the perspective of charge renormalization theories [61], which were originally developed to understand how the surface charge of hard colloids is renormalized due to the presence of ions and other particles with their double layers in suspension.

In this context, there is a maximum effective surface charge that is feasible within the Debye-Hückel approximation, which applies when the renormalized charge, which is small, is taken into account in substitution of the surface bare charge of the particles. Hence, there is a corresponding maximum osmotic pressure from those ions that leak out of the particles [62]. This result follows from geometry and the fact that the Coulomb energies generated by the escaping ions cannot get much larger than k_BT [63]. The maximum free charge that is obtained is [62] $\sim 1.75z(d/l_B)^2$, with z the valence of the free ions. In our case, $z = 1$, since the counterions of the VP microgels are Cl^- ions. Considering now that the diameter of the smallest microgel studied is $d = 240$ nm, we find that the maximum number of free ions is of order 10^5, which is larger than the 10^3 we find experimentally. Therefore, our results are within the limits prescribed by charge renormalization theories.

C. $\phi - \zeta$ relationship and microgel shrinkage at high ζ

In compressible-particle suspensions such as microgel suspensions, the particle volume generally depends on ϕ [64]. As a result, quantifying ϕ can be challenging. Yet, it is highly desirable since ϕ is a relevant thermodynamic variable of the system. To do this, we need to determine $v(\phi)$. This can be done at high ρ using small-angle neutron scattering combined with contrast matching techniques [28–30,33,65–68]. Quite generally, in an elastic scattering experiment, the measured intensity contains information on both the architecture and shape of the single scattering object and the particle arrangement in the sample; these are, respectively, related to the form factor, $P(q)$, with q the scattering momentum transfer and the structure factor, $S(q)$. The idea behind contrast matching is to use the difference in neutron-scattering length between hydrogen (-3.74×10^{-15} m) and deuterium (6.67×10^{-15} m) [69] to eliminate the part of the scattered intensity coming from the structure factor. In this case, $S(q) = 1$, and we can directly determine the form factor of the compressible particles in crowded environments, which can be used to further determine how the particle volume changes with ϕ. The advantage of neutron scattering is that the use of deuterated and/or hydrogenated molecules does not significantly change the chemistry of the samples but allows fine tuning of the contrast of the suspensions. Note that in light- or x-ray scattering, tuning the sample contrast requires using different solvents to, for example, change the relative refractive index of the suspension.

Contrast variation in neutron-scattering experiments can be achieved using the so called tracing method or the zero average contrast (ZAC) method. The tracing method consists in suspending a small amount of hydrogenated microgels in a sea of deuterated microgels that are contrast-matched with a H_2O/D_2O mixture [28,29,33]. Therefore, the form factor of the hydrogenated microgels can be probed directly at high concentration and fitted with appropriate models to obtain both the characteristic length scales within the microgels and the microgel radius and suspension polydispersity, which then allows obtaining the microgel volume [29,33].

The ZAC method relies on measuring the scattered intensity of a suspension composed of a 50/50 mixture (by number) of *identical* hydrogenated and deuterated microgels [28,67,68]. It can be shown that once the particles are suspended in a ≈50 wt %–50 wt % mixture of H_2O/D_2O, $S(q) = 1$ and the measured scattered intensity is proportional to the average form factor of the two species mixed in solution [67]. Once this form factor is obtained, the structural information of the particle can be obtained by fitting it with proper models [28,67].

It is important to note that while for the ZAC method the use of identical particles is essential, since an average form factor is measured, in the tracing method this is not necessary since the signal of the deuterated particles is completely contrast-matched. Therefore, in the tracing method, the deuterated particles can be used to crowd compressible microgels with both different sizes [29] and internal architecture to determine their response to crowding [33,65].

In addition to scattering techniques, super-resolution fluorescent microscopy (SRFM) has shown to be a powerful experimental tool to directly image microgels in real space [70–74]. It has to be noted, anyhow, that SRFM requires the fluorescent labeling of the particles. This can be achieved by adding free amines, e.g., using N-(3-aminopropyl)methacrylamide hydrochloride (APMA) as comonomer. Any dye that is amine reactive, such as N-hydroxysuccinimide (NHS) ester varieties, can be added at a later stage [72]. Whether the additional comonomer changes the crosslinking of the polymeric network and, therefore, the bulk modulus of the microgels, has not yet been investigated. Furthermore, these microscopy techniques require that the observed microgels are immobilized. This can be achieved in a crowded environment [72,73], but in dilute and semidilute conditions the compressible particles must be adsorbed onto a solid substrate [70,71,74]. When soft particles adsorb onto solid substrates they deform [75]. Consequently, the comparison between these measurements and the structure of the particles in bulk is sometimes not that easy.

Another fact that must be considered is that to induce the blinking of the dye, samples for SRFM have to be prepared with the addition of salt, typically mercaptoethylamine [70,72,73], which limits the experimental conditions at which SRFM can be performed.

Finally, we mention that methods to achieve an *in silico* synthesis of microgels have been recently developed [76–79]. In contrast to simulation based on an ideal lattice model, these methods lead to reliable internal structures (with different topology and chain lengths of the polymeric network) and swelling behavior of the simulated microgels [80].

Unfortunately, computer simulations are still limited both in the total size of the microgels that can be simulated and in the number of microgels that can be simulated at the same time. Nevertheless, insights on the particle-to-particle effective interaction potential have already been achieved [81]. These results can be useful to rationalize the variation of the volume of the microgels with increasing packing fraction.

A completely different way to obtain ϕ is to use the measured π and the counterion model accounting for π at relatively low ϕ [48]. The strategy is based on the fact that, experimentally, we measure $\pi = \pi(\zeta)$, while Eq. (8) provides $\pi_c = \pi_c(\phi)$. Since the osmotic pressure is determined by the counterions, $\pi(\zeta) = \pi_c(\phi)$. From the measured π at certain

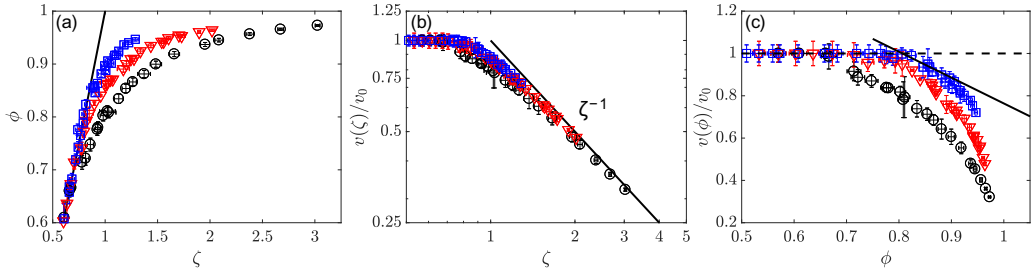

FIG. 9. (a) $\phi - \zeta$ relation obtained from the mapping of the measured osmotic pressure and the model osmotic pressure described by Eq. (8) for VP1, VP4, and VP6 microgels. The solid line corresponds to $\phi = \zeta$. (b) Relative volume change of individual microgels as function of ζ. The solid line is the limiting case, $v(\zeta) \sim \zeta^{-1}$, when only isotropic shrinking happens. (c) Relative volume change as function of ϕ. In all panels: (circles) VP1, (down triangles) VP4, and (squares) VP6 microgels.

ζ, and the model in Eq. (8), we can then map ζ onto ϕ. Figure 9(a) shows this mapping for three suspensions comprised of 2VP microgels with different c_X. Note that $\zeta = \phi$ for ζ up to approximately random close packing, as indicated with the solid line in Fig. 9(a). Interestingly, for $c_X = 1.6\%$ and $c_X = 2.5\%$ the mapping follows this solid line up to $\zeta \sim 0.83$ and ~ 0.78, respectively, indicating that these microgels keep their volume even above random close packing. This behavior is qualitatively reproduced by Monte Carlo simulations of ionic microgels at high packing fractions approximated with the Flory-Rehner theory and interacting via a Hertzian potential [82].

Therefore, at these high concentrations, the microgels first change their shape without appreciable deswelling [72,73,83,84]. This is consistent with crosslinked polymer networks having a shear modulus that is typically much smaller than their bulk modulus [85]. The concave-down shape of the $\phi - \zeta$ data also reflects this fact: the curvature of the $\phi - \zeta$ data reflects its tendency to stay close to the $\phi - \zeta$ line, which corresponds to a lack of compression, emphasizing that changing shape at constant volume is easier than changing volume at constant shape. Interestingly, for the softest microgel ($c_X = 0.2\%$), the deviation from the solid line occurs at a ϕ below which particle-particle contacts are forced due to steric constrains, which is expected for soft particles that shrink due to the osmotic pressure of the ions [29].

Note that in our case, deswelling happens at larger generalized packing fractions compared to prior works with also ionic microgels [25,86]. These other microgels have a similar swelling ratio compared to our microgels; hence, it is reasonable to assume they have a stiffness that is comparable to the stiffness of our particles. The key difference, however, resides in the values of Γ. While the Γ values for our microgels are within 2.2×10^{-3} and 1×10^{-3}, the Γ values in Refs. [25,86] are at least 3×10^{-2}, which is an order of magnitude larger. Hence, counterion-induced deswelling is expected to occur earlier for the ionic microgels used in Refs. [25,86] than for our microgels.

We also note that for $\zeta > 1$, the normalized osmotic pressure shown in Fig. 6 grows much more strongly than linearly. This suggests that the counterions are not uniformly distributed in the suspension volume, as $\pi v_0/(k_B T)$ would grow linearly with ζ in this case; this supports the $\phi - \zeta$ mapping performed, which relies on the fact that the osmotic pressure is determined by the counterions in the free volume outside the microgel particles.

Importantly, though, for $\phi = 1 - \Gamma$, we expect that the osmotic pressure inside the microgels, π_{inside}, becomes equal to the pressure exerted by the counterions, π_c:

$$\Gamma = 1 - \phi \rightarrow \frac{\pi_{\text{inside}} v_0}{k_B T} = Q(1 - \Gamma) = Q\phi$$
$$\frac{\pi_c v_0}{k_B T} = \frac{\Gamma Q \phi}{1 - \phi} = Q\phi = \frac{\pi_{\text{inside}} v_0}{k_B T}. \quad (11)$$

This condition then provides the volume fraction above which counterion-induced deswelling is expected to stop playing a role. It is at the ϕ given by this condition that the counterions become uniformly distributed throughout all the suspension volume. Since Γ is of order 10^{-3} in our case, the corresponding ϕ for this to happen is very high and above those reached in our experiments. Note this also explains why in Ref. [86] a jamming transition is observed after a glass transition; this happens at packing fractions where counterion-induced deswelling no longer has a major effect, allowing steric effects to become dominant in controlling suspension behavior. We have not seen traces of this phenomena in our data.

From the values of ϕ and ζ, we calculate $v/v_0 = \phi/\zeta$ [48]. When plotted versus ζ, we see that v/v_0 decreases for sufficiently large ζ, indicating the microgel compression. We reach the $v(\zeta) \propto \zeta^{-1}$ regime expected for pure isotropic compression at high ζ, as shown by the solid line in Fig. 9(b). Hence, the microgels both change shape and volume at high ζ. There might, however, be some mild interpenetration as the particles both change shape and shrink [72,73,83].

When v/v_0 is plotted against ϕ, Fig. 9(c), the concave-down slope of the data emphasizes again that microgels can more easily change shape than compress. We can also obtain the volume fraction at which the microgel volume begins to shrink, ϕ_s. To determine ϕ_s, we fit a straight line to the 4 points closest to the $v/v_0 = 1$ line having $v(\phi)/v_0 \leqslant 1$, as illustrated in Fig. 9(c) for the VP6 microgels, and calculate the intersection of both lines. We find that within error, ϕ_s is independent of d [see Fig. 10(a)], and thus of c_X and the microgel stiffness.

This can be understood from the fact that for microgel compression to occur, the osmotic pressure must be comparable to the microgel bulk modulus K_p. In our suspensions, π is due

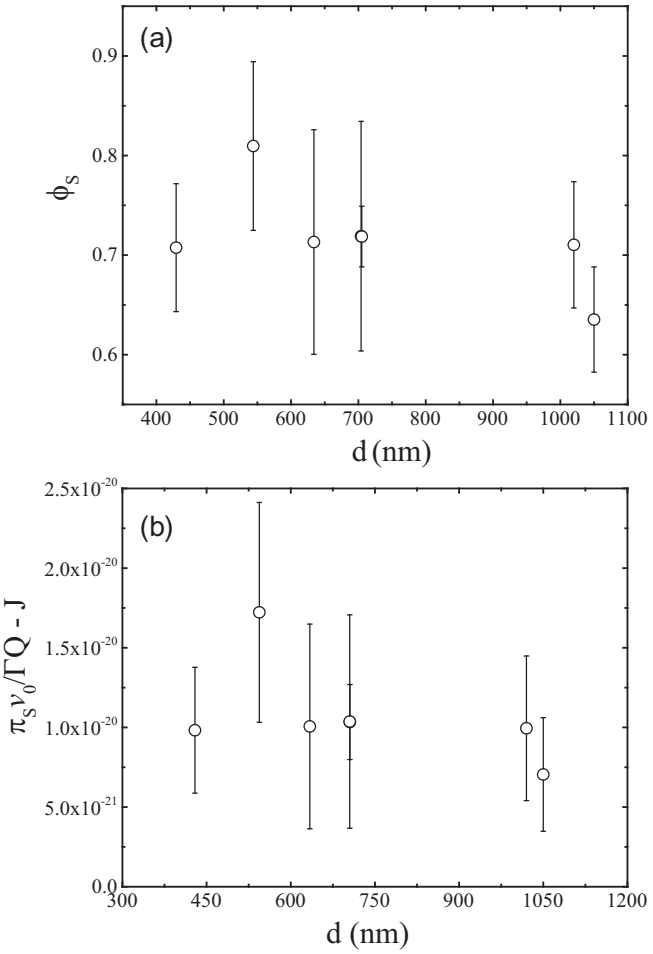

FIG. 10. (a) Packing fraction ϕ_s where microgel shrinking begins as a function of the microgel swollen diameter d. (b) Ratio between the osmotic pressure at which microgels begin to shrink $\pi_S = \pi(\phi_s)$ and the prefactor, $\Gamma Q/v_0$, of π_c.

to the counterions, which scales with d as $\pi_c \propto d^{-5/2}$. The microgel bulk modulus also depends on microgel size; it is an energy density after all. Provided that the characteristic energy scale does not change as the particle compresses, we expect that K_p should scale with d as $K_p \propto d^{-3}$. As a result, the volume fraction where the microgels shrink remain only weakly dependent on d, consistent with the lack of a clear trend in our experimental results. We emphasize that the results are largely independent of the method used to obtain ϕ_s from the v/v_0 versus ϕ curve.

Consistent with the interplay between π and K_p in determining microgel deswelling, we note that the condition $K_p < \pi$ is satisfied in the two cases for which we have measurements of K_p. We previously found that $K_p = (1.6 \pm 0.1)$ kPa for $c_X = 1.3\%$ and (0.4 ± 0.02) kPa for $c_X = 0.5\%$ [40], which are slightly smaller than the pressure at ϕ_s, $\pi_S = \pi(\phi_s) = 2.1 \pm 0.4$ kPa and (1.1 ± 0.4) kPa, respectively. These ideas to understand when microgels compress suggest that the ratio between π_s, corresponding to the osmotic pressure where compression begins, which depends on K_p, and the osmotic pressure, should only show a weak dependence on d and thus on c_X. Consistent with this expectation, $\frac{\pi_S}{\Gamma Q/v_0}$ shows no dependence on d, as shown in Fig. 10(b).

Therefore, it is the balance between the suspension osmotic pressure and the microgel bulk modulus what determines when the microgels appreciably compress. Certainly, for $\phi > \phi_{\rm rcp}$, steric effects should begin to play a role and could potentially compete with counterion-induced deswelling. However, we believe the latter dominates the behavior. To address this, we begin by considering that the magnitude of microgel-microgel interactions will be approximatively given by the single-particle bulk modulus, K_p, times the strain experienced by the microgels, γ. From the literature [40], we know K_p is of order 1 kPa, and that the strain $\gamma = \Delta d/d$, with Δd the change in d, is considerably small. Hence $K_p\gamma < \pi_c$ and steric effects are expected to play a secondary role compared to counterion-induced deswelling, indicating that the suspension osmotic pressure is essentially equal to π_c, even at values of packing fraction above random close packing.

Finally, the constancy of $\pi_S v_0/(\Gamma Q)$ in Fig. 10(b), suggests that when v_0 decreases, corresponding to more crosslinked microgels, ΓQ must also decrease. Since the value of Q is constant, irrespective of c_X, we conclude that Γ is smaller for larger c_X. This fact could be exploited in applications where counterion-induced deswelling is not desireable, and large particle volume fractions are desired with the least number of microgel particles; this could allow, for example, achieving changes in suspension rheology with less amount of material compared to what would be needed if counterion-induced deswelling was at play.

D. Improved model for the counterion osmotic pressure

The initial assumption in the counterion model is that Γ is independent of ζ. This is not true at high concentrations, where, as we have seen, the volume of the microgel is not constant. As a result, Γ changes. We then follow an iterative procedure to obtain $\Gamma(\zeta)$ from the $v = v(\zeta)$ obtained in the previous section, where we assumed Γ was constant, and iteratively repeat the process until the answer converges.

We then start with a constant Γ for $v = v_0$, shown in Fig. 11(a) with a dashed line, an associated fit of the experimental π to Eq. (8), shown with the solid black line in Fig. 11(b), the $\phi - \zeta$ relation, shown with circles in Fig. 11(c), and the $v = v(\phi)$ curve, shown with circles in Fig. 11(d). We then take the $v(\phi)$ obtained, and calculate $\Gamma(\phi)$ using $\Gamma(v) = (\frac{9}{2\sqrt{\pi}})^{1/3}\frac{v^{1/3}}{l_B Q}$, where we have substituted $\kappa^{-1} = 0.5\sqrt{\frac{v}{\pi l_B Q}}$. The result is shown with triangles in Fig. 11(a). We find that Γ/v changes by a factor of $\sim$2 with respect to the initial Γ.

We then calculate π_c using

$$\pi_c = k_B T \frac{\Gamma(v) Q}{v} \frac{\phi}{1-\phi} \tag{12}$$

and obtain that the difference between the new π_c and the initial one is not large, as shown with a blue line in Fig. 11(b). The resultant change in the $\pi - \zeta$ mapping and $v(\phi)$ relation is shown with triangles in Figs. 11(b)–11(d). A third iteration leaves the result unchanged [squares in Fig. 11(a) and red line in Fig. 11(b)]. Note that the $\phi - \zeta$ and $v(\phi)$ relation remain qualitatively unchanged, suggesting the conclusions from the

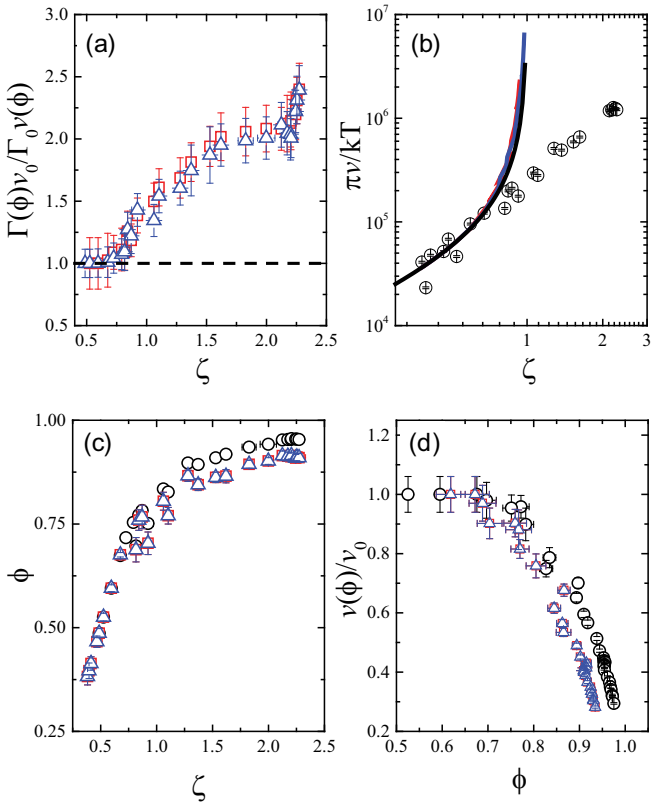

FIG. 11. (a) Normalized fraction of unbounded counterions times the microgel volume versus ζ after two iterations using Eq. (12). The dashed line corresponds to the initial condition for the iterative model. The triangles are the results after the first iteration while the squares correspond to the results after the second iteration. (b) Osmotic pressure for suspensions comprised of VP5 microgels and fits obtained after each iteration. (c) $\phi - \zeta$ mapping for each iteration. (d) Relative volume change as a function of packing fraction for each iteration. In panels (c) and (d), circles, triangles, and squares correspond to the initial condition, and the first and second iterations, respectively.

simpler analysis in the previous section remain essentially unchanged [squares versus triangles in Figs. 11(c) and 11(d)].

V. CONCLUSIONS

We have performed careful dialysis to obtain the osmotic pressure of microgel suspensions and compared the results with those obtained using membrane osmometry, finding excellent agreement between the two. In doing so, we have presented basic thermodynamic aspects on how π is related to the solvent chemical potential, and used these ideas to understand the behavior of ionic-microgel suspensions. Our mesasurements indicate that the free ions in solution control the osmotic pressure of the suspensions. Note that this is true for ionic microgels (with charges distributed along all the polymeric networks) but also for neutral microgels since they possess charges in the particle periphery due to the polar initiator used in the precipitation polymerization synthesis [53]. This is particularly important for microgel suspensions since microgels are compressible and can shrink in response to an unbalanced osmotic pressure inside and outside the particles [29,45,59,60,78].

By combining membrane osmometry and dialysis results, we have proven the significance of the Donnan equilibrium conditions as well as the consistency with charge renormalization ideas [61,63]. From the experiments, we have used π to obtain how ϕ depends on ζ. This approach further allows determining the volume change of the microgels as a function of packing fraction, which depends on the mechanical properties of particles; the shape of the microgel volume versus ϕ curves we have obtained indicates that these particles can change shape more easily than they can compress, and thus have a shear modulus that is smaller than the bulk modulus. A similar behavior has been observed for larger microgels visualized in a confocal microscope [83].

Our model can further be used to explore the role of osmotic pressure and osmotic deswelling in affecting the shape of different microgel particles. Recent advances in the synthetic protocols allow obtaining microgels with different internal structures, including hollow microgels, which are polymeric networks with a solvent-filled cavity in their center. Similar to regular microgels, these hollow soft particles can be synthesized with both charges along all the polymer backbone (ionic hollow microgels) [87] or with charges solely concentrated at the external periphery of the shells and that are due to the polar initiators used in the synthesis (neutral hollow microgels) [33]. Recent results have shown that the swelling toward and away from the internal cavity can be tuned by salt or microgel concentration [65,87]; these effects are definitively related to the suspension osmotic pressure and, therefore, as demonstrated here, to the concentration of ions in suspension.

Finally, we mention that even in suspensions of microgels considered neutral, the osmotic pressure is governed at low concentrations by the free ions derived from the polar initiator used in the synthesis. This means that the use of, namely, neutral microgels as model systems for truly soft spheres must be carefully analyzed to fully understand which properties in their phase behavior are due to the structural softness and which properties are due to ionic effects. These problems can be better studied and rationalized either by developing new model systems for truly neutral and soft spheres, for example, by using an apolar initiator, or by dramatically minimizing the amount of charges incorporated to the microgel periphery.

ACKNOWLEDGMENTS

We thank MCIU/AEI/FEDER, UE (Grant No. PGC2018-336 097842-B-I00), the Deutsche Forschungsgemeinschaft within project A3 (Project No. 191948804) of the SFB 985—Functional Microgels and Microgel Systems, and the SNF (Grant No. 200020_184839). We are also thankful to L. Andrew Lyon for the synthesis of the pNIPAM particles.

[1] P. N. Pusey and W. Van Megen, Nature **320**, 340 (1986).
[2] A. van Veluwen, H. N. Lekkerkerker, C. G. de Kruif, and A. Vrij, Faraday Discuss. Chem. Soc. **83**, 59 (1987).
[3] P. Pusey, H. Lekkerkerker, E. Cohen, and I. De Schepper, Physica A **164**, 12 (1990).
[4] H. N. Lekkerkerker, W.-K. Poon, P. N. Pusey, A. Stroobants, and P. Warren, EPL (Europhys. Lett.) **20**, 559 (1992).
[5] P. Pusey, W. C. Poon, S. Ilett, and P. Bartlett, J. Phys.: Condens. Matter **6**, A29 (1994).
[6] W. C. Poon, Curr. Opin. Colloid Interface Sci. **3**, 593 (1998).
[7] U. Gasser, E. R. Weeks, A. Schofield, P. Pusey, and D. Weitz, Science **292**, 258 (2001).
[8] W. Poon, Science **304**, 830 (2004).
[9] U. Gasser, J. Phys.: Condens. Matter **21**, 203101 (2009).
[10] W. C. Poon, E. R. Weeks, and C. P. Royall, Soft Matter **8**, 21 (2012).
[11] N. F. Carnahan and K. E. Starling, J. Chem. Phys. **51**, 635 (1969).
[12] T. G. Mason, J. Bibette, and D. A. Weitz, Phys. Rev. Lett. **75**, 2051 (1995).
[13] B. J. Ackerson, S. E. Paulin, B. Johnson, W. van Megen, and S. Underwood, Phys. Rev. E **59**, 6903 (1999).
[14] V. Trappe, V. Prasad, L. Cipelletti, P. Segre, and D. A. Weitz, Nature **411**, 772 (2001).
[15] P. Pusey, E. Zaccarelli, C. Valeriani, E. Sanz, W. C. Poon, and M. E. Cates, Philos. Trans. R. Soc. A **367**, 4993 (2009).
[16] H. Princen, J. Colloid Interface Sci. **71**, 55 (1979).
[17] T. G. Mason and J. Bibette, Phys. Rev. Lett. **77**, 3481 (1996).
[18] M.-D. Lacasse, G. S. Grest, D. Levine, T. G. Mason, and D. A. Weitz, Phys. Rev. Lett. **76**, 3448 (1996).
[19] E. B. Sirota, H. D. Ou-Yang, S. K. Sinha, P. M. Chaikin, J. D. Axe, and Y. Fujii, Phys. Rev. Lett. **62**, 1524 (1989).
[20] B. V. R. Tata, P. S. Mohanty, and M. C.Valsakumar, Phys. Rev. Lett. **88**, 018302 (2001).
[21] P. Bartlett and A. I. Campbell, Phys. Rev. Lett. **95**, 128302 (2005).
[22] A. Fernandez-Nieves and A. M. Puertas, *Fluids, Colloids, and Soft Materials: An Introduction to Soft Matter Physics* (Wiley Online Library, Hoboken, New Jersey, 2016).
[23] T. Biben and J.-P. Hansen, J. Phys.: Condens. Matter **6**, A345 (1994).
[24] A. P. Philipse and G. H. Koenderink, Adv. Colloid Interface Sci. **100**, 613 (2003).
[25] R. Borrega, M. Cloitre, I. Betremieux, B. Ernst, and L. Leibler, EPL (Europhys. Lett.) **47**, 729 (1999).
[26] A. S. J. Iyer and L. A. Lyon, Angew. Chem. **121**, 4632 (2009).
[27] G. Romeo, L. Imperiali, J.-W. Kim, A. Fernández-Nieves, and D. A. Weitz, J. Chem. Phys. **136**, 124905 (2012).
[28] U. Gasser, J. Hyatt, J.-J. Lietor-Santos, E. Herman, L. A. Lyon, and A. Fernandez-Nieves, J. Chem. Phys. **141**, 034901 (2014).
[29] A. Scotti, U. Gasser, E. S. Herman, M. Pelaez-Fernandez, L. A. Lyon, and A. Fernandez-Nieves, Proc. Natl. Acad. Sci. **113**, 5576 (2016).
[30] A. Scotti, U. Gasser, E. S. Herman, J. Han, A. Menzel, L. A. Lyon, and A. Fernandez-Nieves, Phys. Rev. E **96**, 032609 (2017).
[31] J. Brijitta and P. Schurtenberger, Curr. Opin. Colloid Interface Sci. **40**, 87 (2019).
[32] A. Ghosh, G. Chaudhary, J. G. Kang, P. V. Braun, R. H. Ewoldt, and K. S. Schweizer, Soft Matter **15**, 1038 (2019).
[33] A. Scotti, A. R. Denton, M. Brugnoni, J. E. Houston, R. Schweins, I. I. Potemkin, and W. Richtering, Macromolecules **52**, 3995 (2019).
[34] H. G. Schild, Prog. Polym. Sci. **17**, 163 (1992).
[35] A. Loxley and B. Vincent, Colloid Polym. Sci. **275**, 1108 (1997).
[36] T. Hoare and R. Pelton, Macromolecules **37**, 2544 (2004).
[37] M. Stieger, W. Richtering, J. S. Pedersen, and P. Lindner, J. Chem. Phys. **120**, 6197 (2004).
[38] R. Keidel, A. Ghavami, D. M. Lugo, G. Lotze, O. Virtanen, P. Beumers, J. S. Pedersen, A. Bardow, R. G. Winkler, and W. Richtering, Sci. Adv. **4**, eaao7086 (2018).
[39] J. Oberdisse and T. Hellweg, Colloid Polym. Sci. **298**, 921 (2020).
[40] B. Sierra-Martin, J. A. Frederick, Y. Laporte, G. Markou, J. J. Lietor-Santos, and A. Fernandez-Nieves, Colloid Polym. Sci. **289**, 721 (2011).
[41] B. Sierra-Martin and A. Fernandez-Nieves, Soft Matter **8**, 4141 (2012).
[42] H. Senff and W. Richtering, J. Chem. Phys. **111**, 1705 (1999).
[43] M. Clements, S. R. Pullela, A. F. Mejia, J. Shen, T. Gong, and Z. Cheng, J. Colloid Interface Sci. **317**, 96 (2008).
[44] D. Paloli, P. S. Mohanty, J. J. Crassous, E. Zaccarelli, and P. Schurtenberger, Soft Matter **9**, 3000 (2013).
[45] T. J. Weyer and A. R. Denton, Soft Matter **14**, 4530 (2018).
[46] M. J. Bergman, N. Gnan, M. Obiols-Rabasa, J.-M. Meijer, L. Rovigatti, E. Zaccarelli, and P. Schurtenberger, Nat. Commun. **9**, 5039 (2018).
[47] A. Scotti, S. Bochenek, M. Brugnoni, M.-A. Fernandez-Rodriguez, M. F. Schulte, J. Houston, A. P. Gelissen, I. I. Potemkin, L. Isa, and W. Richtering, Nat. Commun. **10**, 1418 (2019).
[48] M. Pelaez-Fernandez, A. Souslov, L. A. Lyon, P. M. Goldbart, and A. Fernandez-Nieves, Phys. Rev. Lett. **114**, 098303 (2015).
[49] P. Atkins and J. De Paula, *Elements of physical chemistry* (Oxford University Press, USA, 2013).
[50] P. J. Flory, *Principles of Polymer Chemistry* (Cornell University Press, Ithaca, London, 1953).
[51] B. J. Berne and R. Pecora, *Dynamic Light Scattering: With Applications to Chemistry, Biology, and Physics* (Courier Corporation, Moneola, New York, 2000).
[52] A. Fernández-Nieves, A. Fernández-Barbero, B. Vincent, and F. De Las Nieves, Macromolecules **33**, 2114 (2000).
[53] R. Pelton and P. Chibante, Colloids Surf. **20**, 247 (1986).
[54] M. Andersson and S. L. Maunu, J. Polym. Sci., Part B: Polym. Phys. **44**, 3305 (2006).
[55] C. Bonnet-Gonnet, L. Belloni, and B. Cabane, Langmuir **10**, 4012 (1994).
[56] A. Fernández-Nieves, A. Fernández-Barbero, B. Vincent, and F. De las Nieves, J. Chem. Phys. **119**, 10383 (2003).
[57] M. C. Wilkinson, J. Hearn, and P. A. Steward, Adv. Colloid Interface Sci. **81**, 77 (1999).
[58] R. van Roij, J. Phys.: Condens. Matter **15**, S3569 (2003).
[59] U. Gasser, A. Scotti, and A. Fernandez-Nieves, Phys. Rev. E **99**, 042602 (2019).
[60] A. R. Denton and Q. Tang, J. Chem. Phys. **145**, 164901 (2016).
[61] S. Alexander, P. Chaikin, P. Grant, G. Morales, P. Pincus, and D. Hone, J. Chem. Phys. **80**, 5776 (1984).
[62] M. J. Stevens, M. L. Falk, and M. O. Robbins, J. Chem. Phys. **104**, 5209 (1996).

[63] M. Stevens and M. Robbins, Europhys. Lett. **12**, 81 (1990).
[64] J. R. Seth, L. Mohan, C. Locatelli-Champagne, M. Cloitre, and R. T. Bonnecaze, Nat. Mater. **10**, 838 (2011).
[65] A. Scotti, M. Brugnoni, A. Rudov, J. Houston, I. Potemkin, and W. Richtering, J. Chem. Phys. **148**, 174903 (2018).
[66] G. D. Wignall and Y. B. Melnichenko, Rep. Prog. Phys. **68**, 1761 (2005).
[67] P. S. Mohanty, S. Nöjd, K. v. Gruijthuijsen, J. J. Crassous, M. Obiols-Rabasa, R. Schweins, A. Stradner, and P. Schurtenberger, Sci. Rep. **7**, 1487 (2017).
[68] S. Nöjd, P. Holmqvist, N. Boon, M. Obiols-Rabasa, P. S. Mohanty, R. Schweins, and P. Schurtenberger, Soft Matter **14**, 4150 (2018).
[69] F. S. Varley, Neutron News **3**, 26 (1992).
[70] A. P. Gelissen, A. Oppermann, T. Caumanns, P. Hebbeker, S. K. Turnhoff, R. Tiwari, S. Eisold, U. Simon, Y. Lu, J. Mayer, *et al.*, Nano Lett. **16**, 7295 (2016).
[71] S. Bergmann, O. Wrede, T. Huser, and T. Hellweg, Phys. Chem. Chem. Phys. **20**, 5074 (2018).
[72] G. M. Conley, P. Aebischer, S. Nöjd, P. Schurtenberger, and F. Scheffold, Sci. Adv. **3**, e1700969 (2017).
[73] G. M. Conley, C. Zhang, P. Aebischer, J. L. Harden, and F. Scheffold, Nat. Commun. **10**, 2436 (2019).
[74] P. Otto, S. Bergmann, A. Sandmeyer, M. Dirksen, O. Wrede, T. Hellweg, and T. Huser, Nanoscale Adv. **2**, 323 (2020).
[75] M. F. Schulte, A. Scotti, M. Brugnoni, S. Bochenek, A. Mourran, and W. Richtering, Langmuir **35**, 14769 (2019).
[76] N. Gnan, L. Rovigatti, M. Bergman, and E. Zaccarelli, Macromolecules **50**, 8777 (2017).
[77] S. Nikolov, A. Fernandez-Nieves, and A. Alexeev, Appl. Math. Mech. **39**, 47 (2018).
[78] G. Del Monte, A. Ninarello, F. Camerin, L. Rovigatti, N. Gnan, and E. Zaccarelli, Soft Matter **15**, 8113 (2019).
[79] A. A. Gavrilov, V. Y. Rudyak, and A. V. Chertovich, J. Colloid Interface Sci. **574**, 393 (2020).
[80] L. Rovigatti, N. Gnan, and E. Zaccarelli, J. Phys.: Condens. Matter **30**, 044001 (2017).
[81] L. Rovigatti, N. Gnan, A. Ninarello, and E. Zaccarelli, Macromolecules **52**, 4895 (2019).
[82] M. Urich and A. R. Denton, Soft Matter **12**, 9086 (2016).
[83] I. Bouhid de Aguiar, T. van de Laar, M. Meireles, A. Bouchoux, J. Sprakel, and K. Schroën, Sci. Rep. **7**, 10223 (2017).
[84] S. V. Nikolov, A. Fernandez-Nieves, and A. Alexeev, Proc. Natl. Acad. Sci. **117**, 27096 (2020).
[85] P. Voudouris, D. Florea, P. van der Schoot, and H. M. Wyss, Soft Matter **9**, 7158 (2013).
[86] C. Pellet and M. Cloitre, Soft Matter **12**, 3710 (2016).
[87] S. K. Wypysek, A. Scotti, M. O. Alziyadi, I. I. Potemkin, A. R. Denton, and W. Richtering, Macromol. Rapid Comun. **41**, 1900422 (2020).